ORIGINAL PAPER

Application of multifractal modeling technique in systematic lithogeochemical survey to identify Au–Cu anomalies in the Siah-Jangal area, Southeastern of Iran

Zahra Mokhtari · Mohammad Boomeri · Sasan Bagheri

Abstract Identifying the geochemical anomalies from background is a fundamental task in exploration geochemistry. This research is based on the application of concentration–area (C–A) method at the Siah-Jangal Au porphyry system in southeastern Iran. Lithogeochemical datasets ($n=399$) were used in this geochemical survey which was conducted for the exploration for Au mineralization. Moreover, similar surveys were also carried out for As, Cu, and Mo exploration in this region. Anomalous threshold values for the mineralized zone were computed and compared with the statistical methods based on the data obtained from chemical analysis of samples for the lithological units. Several anomalies at a local scale were identified for Au (281 ppb), As (649 ppm), and Cu (20 ppm). The obtained results suggest existence of local Au anomalies that its magnitude generally is above 400 ppb. The C–A log–log plots show existence of three stages of Au and Cu enrichment. The second and most important enrichment event is responsible for the presence of Au at grades above 400 ppb. The obtained results have been interpreted using rather extensive set of information available for the study area, consisting of structural interpretation and alteration data. Various structural features and corresponding alteration show that the geologic structures play an important role in the discrimination of geochemical anomalies and element distribution in the Siah-Jangal area.

Z. Mokhtari (✉) · M. Boomeri · S. Bagheri
Department of Geology, Faculty of Sciences,
University of Sistan and Baluchestan, Zahedan, Iran
e-mail: Zahra.mokhtari1985@gmail.com

Introduction

The Separation of geochemical anomalies from background values in areas is one of the most fundamental tasks in the fields of mineral exploration and mineral resource assessment. Since geochemical elements can provide important and direct clues related to the presence of mineral deposits, geochemical anomalies will continue playing an important role in mineral exploration (Cheng et al. 1994; Cheng 1999; Grunsky and Smee 1999; Harris et al. 1999, 2000; Chen et al. 2001; Singer and Kouda 2001). In the past recent years, geochemical anomalies have been identified by means of various methods. Some of these processing methods come from the developments of theoretical geostatistics, and other from the theory of multifractals (e.g., Carranza 2008; Deng et al. 2010; Afzal et al. 2011, 2013, 2014; Pazand et al. 2011; Cheng 2012; Hashemi and Afzal 2013; Wang et al. 2012; Zuo 2011; Zuo et al. 2012).

The statistical methods have been widely used to determine threshold values separating background populations from anomalies (e.g., Carranza 2008; Zuo 2011; Cheng 2012). These methods are only applicable to cases that the geochemical data follows a normal distribution. Moreover, statistical methods e.g., by histogram analysis or Q–Q plots assuming normality or log normality and do not consider the shape, extent and magnitude of anomalous and geological environments areas (Rafiee 2005) and therefore may fail to recognize anomalies in regions with high background values close to anomalous values, or miss weak anomalies in regions with known mineral deposits (Hassanpour and Afzal 2011).

Fractal theory is one of the non-linear mathematics which considers the geometry property of geochemical landscape and established by Mandelbrot (1983). The word "Fractal" is driven from the Latin word "fractus", meaning broken, which utilized for the objects that were too irregular to be

described by ordinary Euclidean geometry. In the geological sciences, these approaches have been used to describe the irregularity of geological features and the spatial distribution patterns of geological objects (i.e., Zuo et al. 2009; Gumiel et al. 2010). Several different fractal and multifractal models have been proposed to assess element concentration and determine thresholds of geochemical anomalies. Examples include the concentration–area model (C–A) (Cheng et al. 1994), the spectrum–area model (S–A) (Cheng 2000), the multifractal singular value decomposition (MSVD) (Li and Cheng 2004), the concentration–distance (C–D) model (Li et al. 2003), the mapping singularity technique (Cheng 2007, 2008; Arias et al. 2012) and many other applications (e.g., in the environmental field; Lima et al. 2003, 2008). Among these, the Concentration–Area (C–A) method, proposed by Cheng et al. (1994), is based on the premise that geochemical distributions reflect multifractal property in nature but only few applications have been reported in the literature. Few authors put forward this idea and explain its vast applications (Goncalves et al. 1998; Cheng 1999, 2008; Sim et al. 1999; Wei and Pengda 2002; Zuo et al. 2009; Afzal et al. 2010; Arias et al. 2012).

In this paper, after a brief discussion of the "concentration–area" method, the application of multifractal modeling in a systematic lithogeochemical survey for identifying areas potentially favorable for Au and Cu are described. For demonstration purposes, the Siah-Jangal area, North of Taftan volcano, southeast Iran, will be studied as an example.

The concentration–area method for geochemical anomaly separation

The concentration–area fractal model is used for illustrating the relationship between the obtained results and the geological, geochemical, and mineralogical information for discrimination of anomalies from background in geochemical and geophysical exploration. Its most useful features are the easy implementation and the ability to compute quantitative anomalous thresholds (Goncalves et al. 1998). The fractal concentration–area (C–A) model originally proposed by Cheng et al. (1994) is based on an empirical set of equations, which may be used to define the geochemical background and anomalies. This model has the general form:

$$A(\rho \leq \nu) \propto \rho^{-a1}; A(\rho \geq \nu) \propto \rho^{-a2} \qquad (1)$$

Where $A(\rho \leq \nu)$ and $A(\rho \geq \nu)$ denote the areas (A) with concentration values ρ that are respectively smaller and greater than the contour value ρ; ν represents the threshold; and a_1 and a_2 are characteristic exponents for both criteria. Using fractal theory, Cheng et al. (1994) obtained similar power–law relationships and equations in extended form. The two approaches which were used to calculate $A(\rho)$ by Cheng et al. (1994) were: (1) the $A(\rho)$ is the area enclosed by contour level q on a geochemical contour map resulting from interpolation of the original data using a weighted moving average method, and (2) $A(\rho)$ are the values obtained by box counting of original elemental concentration values. By box counting, one


Fig. 1 Regional geotectonic setting of the Makran arc-trench system and Neogen Baluchistan volcanic arc (Based on Grando and McClay 2007; Ellouz-Zimmermann et al. 2007)
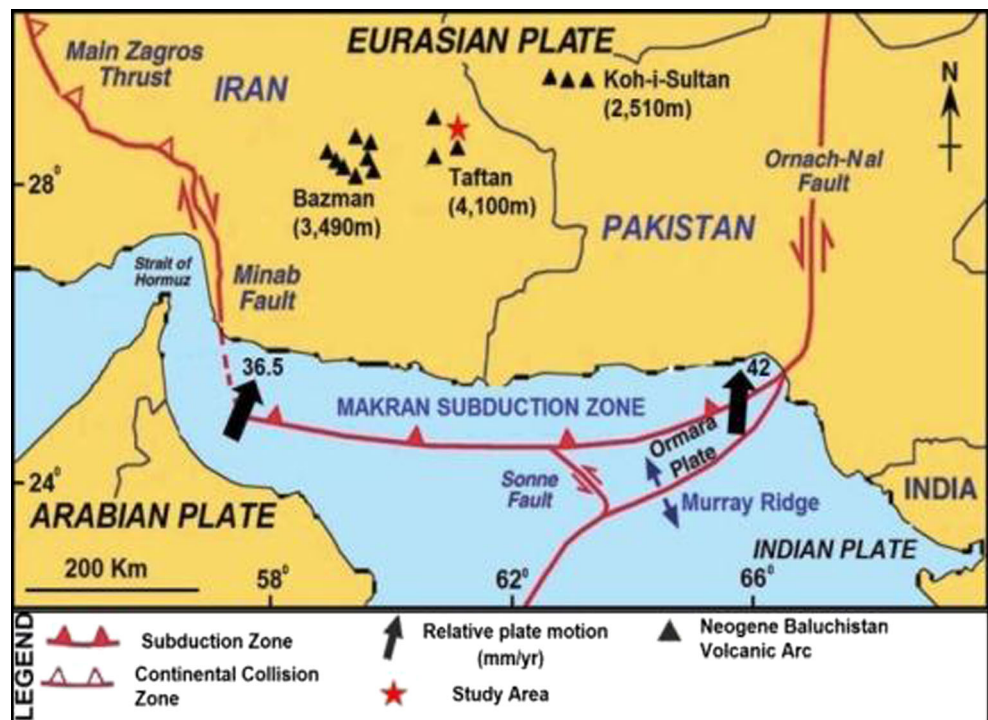
superimposes grid with cells on the study region. The area $A(\rho)$ for a given q is equal to the number of cells multiplied by cell area with concentration values greater than ρ. Average concentration values are used for those boxes containing more than one sample. Area–concentration $[A(\rho)]$ with element concentrations greater than ρ usually shows a power–law relation (Cheng et al. 1994). The breaks between straight-line segments on this plot and the corresponding values of ρ have been used as cut-offs to separate geochemical values into different components, representing different causal factors, such

as lithological differences and geochemical processes (Carranza 2009; Afzal et al. 2010). Factors such as mineralizing events, surface geochemical element concentrations, and surface weathering are of considerable importance (Lima et al. 2003). Multifractal theory can be interpreted as a theoretical framework that explains the power–law relations between areas enclosing concentrations below a given value and the actual concentrations. Extensive computation is required for demonstrating and proving that data distribution has a multifractal nature. This method has several limitations and

Fig. 2 Geological sketch map of the Siah-Jangal and surrounding area; *1*, *A* andesitic tuff, *B* dacite and andesitic lava flows, other color: quaternary alluvial plains; *2 A* mudstone and shale; *B* gray fossiliferous limestone; *C* meta greywacke; *D* pelitic shale with thin zlava flow of basalt and red shale; *3 A* flysh; *B* red shale and argillaceous phyllite; *C* sandstone; *D* pelitic shale in association with abundant lava flow of basalt; *4 A* serpentinite; *B* spilitic rocks; *C* colored melange characterized by an ultrabasic matrix (Modified after Mehrpartoo and Padiar 2003)
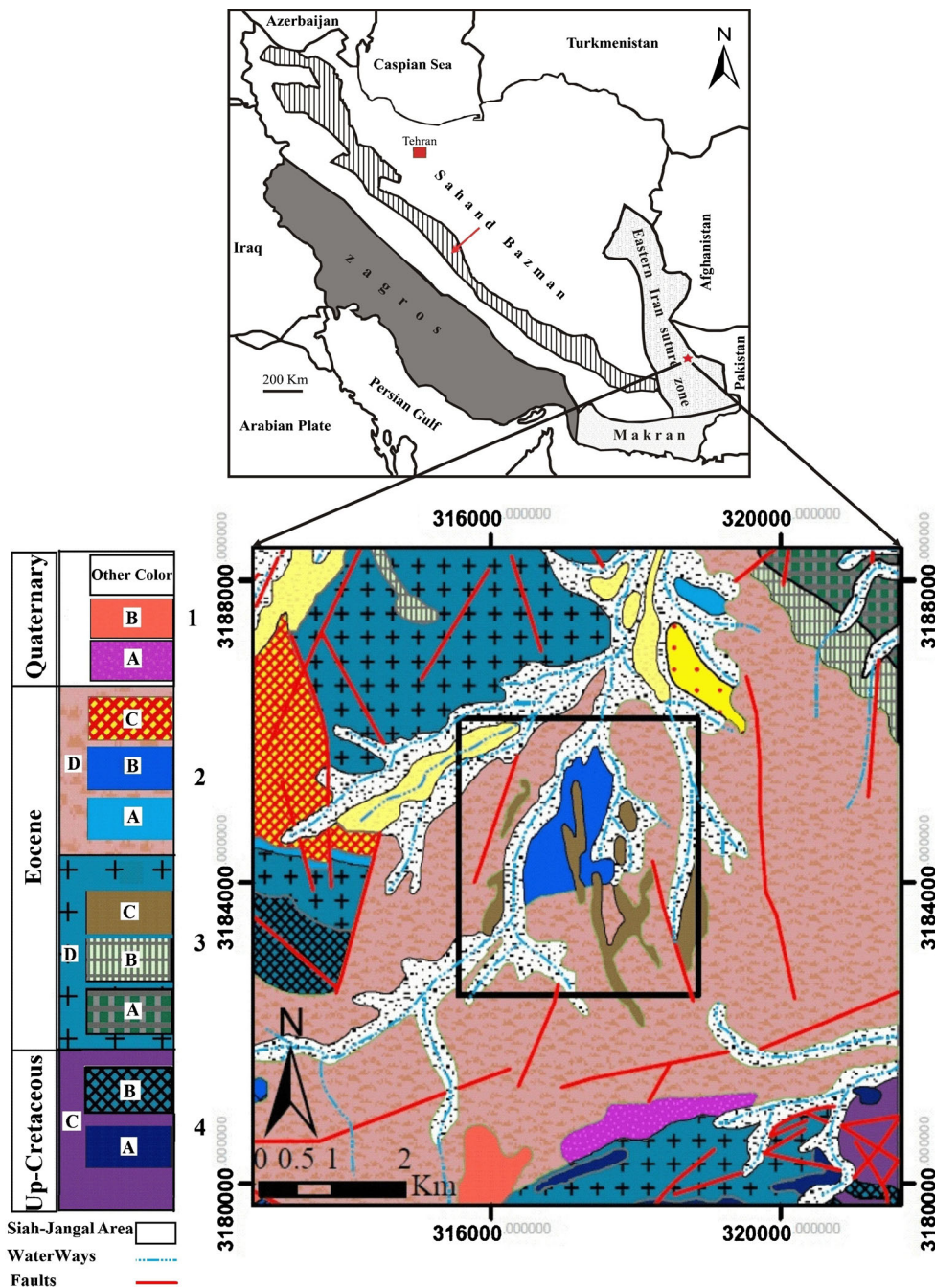
accuracy problems, especially when the boundary effects on irregular geometrical datasets are involved (Agterberg et al. 1996; Li et al. 2003). The C–A method seems to be equally applicable as well to all cases, which is probably in consequence of the fact that geochemical distributions mostly satisfy the properties of a multifractal function. There are some evidence that geochemical distributions are fractal in nature and behavior, at least empirically according to Bolviken et al. (1992). Although there is some debate, most authors support the multifractality of the geochemical distributions (Cheng and Agterberg 1996; Turcotte 1997; Goncalves et al. 2001; Li et al. 2003; Afzal et al. 2010; Pazand et al. 2011). This idea may provide and help the development of an alternative interpretation validation and useful methods to be applied for elemental geochemical distributions analysis.

Geological setting

The Siah-Jangal area is situated in the north of Taftan volcano in southeastern Iran. The volcanic centers of Taftan and Bazman in Iran and Sultan in Pakistan were formed by the subduction of the Oman oceanic crust under the southern margin of the Makran zone (Farhoudi and Karige 1997; Berberian et al. 1982). This volcanic belt extends through an E-W belt developed from the Bazman volcano in Iran to Sultan in Pakistan and made a classic magmatic arc parallel to the Makran Zone (Northern Makran magmatic arc or NMA). The NMA is bounded in the west to Sahand–Bazman magmatic belt and in the east to Ornach-Nal fault zones and Himalaya Mountains (Fig. 1). There are many intrusive rocks that occur in the same direction with the NMA such as Cretaceous Bazman granitoid in north of the Mount Bazman. Moreover the Mount Taftan was constructed on a basement which has many Eocene and Miocene stocks and dykes. Existence of these rocks is thought to be related to the younger magmatism episode that either was originated by subduction of the Oman Ocean under the Makran zone (Berberian et al. 1982) or a syn- to postcollision magmatism link to closuring event of the Sistan Ocean (Tirrul et al. 1983).

In Pakistanian part of NMA just close to Iran boundary, there are numerous Cu mineralizations at Saindak and Reko Diq (Rowan et al. 2006; Perello et al. 2008). In Iranian part of NMA, especially in the northern slope of the Taftan volcano, where in the Siah-Jangal area; there is a wide range of hydrothermal alteration and mineralization related to the mentioned magmatic event/s. This area has great potentials for mineral exploration and prospecting for Cu and Au porphyry and other epithermal deposits. Ancient underground mining shows that mineral veins were known 100 years ago. The recent
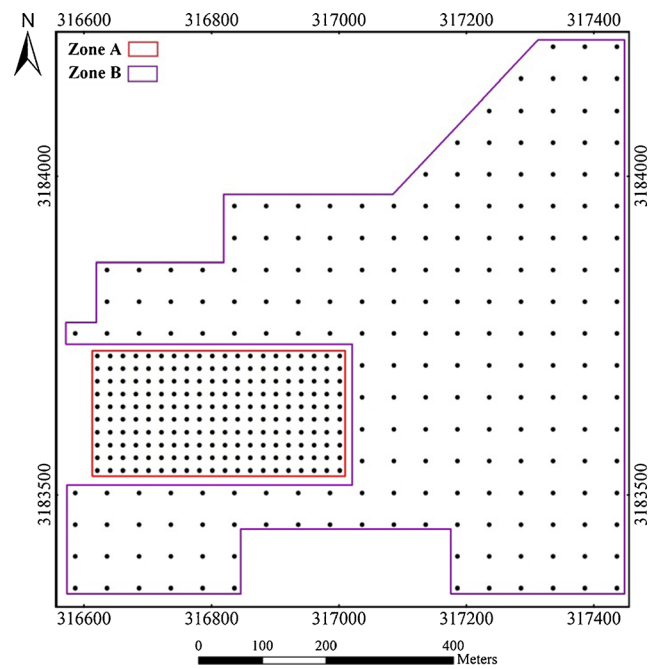

Fig. 3 Lithogeochemical samples' location map of Siah-Jangal area

geological and mineralogical studies were presented by Taghizadeh (1996), Zarcan Company (2003), and Kavoshgaran Company (2003, 2006). There is a thick mineralized silicic vein in the central part of the study area which is surrounded by phyllic, argillic, and propylitic alteration zones. Moreover, quartz in the silicic vein contains polyphase and vapor-rich fluid inclusions. Salinity of the polyphase fluid inclusions is very high (up to 80 wt.% equivalent NaCl). The homogenization temperatures for this type are also high up to more than 500 °C. The fluid inclusions in the quartz have characteristics of those which were described for porphyry ore deposits. A simplified geological map of the Siah-Jangal area is presented in Fig. 2. The oldest rocks outcropped in this area

Table 1 Statistical parameters of raw data based on lithogeochemical samples analysis in the Siah-Jangal area

	Cu (ppm)	Au (ppb)	As (ppm)	Mo (ppm)
Mean	33.85	225.22	827.32	1.54
Median	24.60	16.00	75.90	1.40
Standard deviation	31.41	1127.94	4198.37	0.86
Variance	986.90	1,272,248.03	17,626,318.11	0.74
Skewness	2.87	9.11	8.54	4.32
Kurtosis	10.19	90.92	77.74	29.55
Minimum	4.60	0.00	0.00	0.30
Maximum	229.00	13,900.00	47,300.00	9.00

Table 2 Results of Shapiro–Wilk testing of lithogeochemical data from the Siah-Jangal area

Shapiro–Wilk			
	Statistic	df	Significance
Au	0.175	399	0.000
As	0.172	399	0.000
Cu	0.689	399	0.000
Mu	0.668	399	0.000

are mainly siliciclastic deposits and serpentinite and spilitic rocks, which are part of the flysch zone of eastern Iran. These rocks consist of a thick pelitic and psammitic succession with intercalated basaltic lava flows and radiolarian shales and carbonate, as well as Eocene fossiliferous limestone and greywacke. A younger Pleistocene and Quaternary volcanic rocks consist of tuff, dacite and andesitic lava flows unconformably cover the flysch deposits. Quaternary alluvial

deposits are the youngest exposures in the studied area. There is a strong structural control on essentially all ore deposit types in the Siah-Jangal area. The mentioned rocks have been affected by several faults and fracturing systems; one of the most important of them is the left-lateral strike-slip fault system which transected the flysch zone in an E–W trend through the Junabad village, few kilometers north of the studied area.

Sampling and lithogeochemistry analysis

A total of 399 lithogeochemical samples were collected from the study area, as depicted in Fig. 3. These samples were analyzed by ICP-MS for 44 elements. Concentration values of Au, As, Cu, and Mo are used in this study. These elements were selected due to their utility as pathfinder elements for gold mineralization in a porphyry setting. Detection limits for Au, Cu, As, and Mo are 1 ppb, 0.2 ppm, 0.5 ppm, and
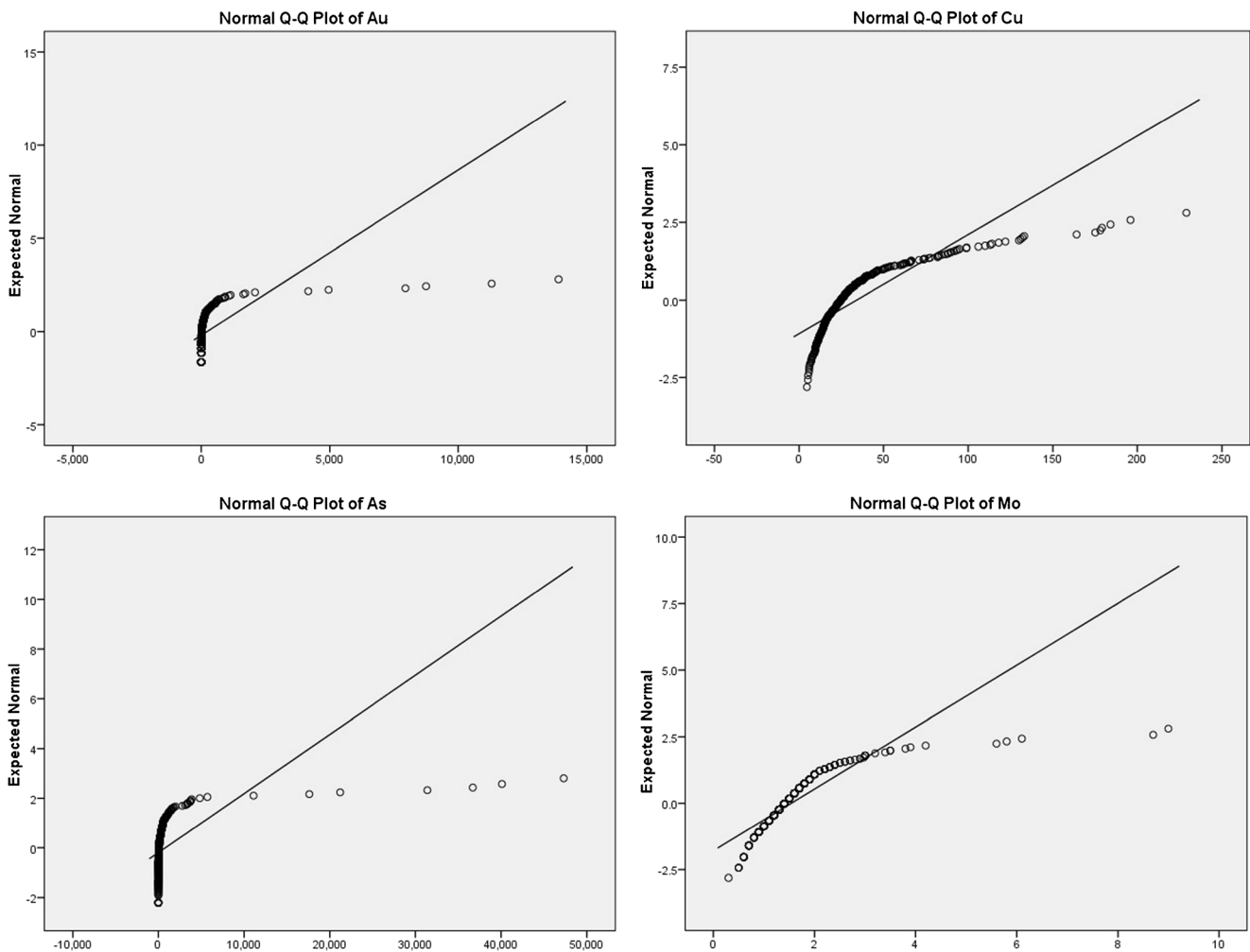

Fig. 4 The Q–Q plots of Au, As, Cu, and Mo showing that elemental concentrations are not normally distributed

0.1 ppm, respectively. The main statistical properties of the lithogeochemical data are summarized in Table 1. The raw dataset is highly spatially variable due to the diversity of geological, lithology, and features such as thrusts, faults, and mineral concurrences (Ford and Blenkinsop 2008). According to this table, Au and Cu mean values are 225 ppb and 33 ppm, respectively. Variations between maximum and minimum for these data reveal a wide range. If median is assumed to be equal to threshold values, the obtained statistical results are 16 ppb for Au, 24 ppm for Cu, 75 ppm for As, and 1 ppm for Mo (see Table 1).

There are several methods of assessing whether data are normally distributed or not. They fall into two broad categories; graphically and statistically. The most common are Shapiro–Wilk test (Shapiro and Wilk 1965) and Q–Q probability plots. Table 2 presents the results from the Shapiro–Wilk test for lithogeochemical samples analysis in Siah-Jangal area. The Shapiro–Wilk test is more appropriate for small sample sizes (<50 samples) and can also handle sample sizes as large as 2000. According to this reason, the Shapiro–Wilk test will

be used as the numerical means of assessing normality. If the significant value of the Shapiro–Wilk test is greater than 0.05, the data is normal, and if it is below 0.05, the data significantly deviate from a normal distribution. As it can be seen from Table 2, significant values of the raw lithogeochemical data for Au, As, Cu, and Mo are indicating that the data are non-normally distributed.

The Q–Q plot of a uni-element data can be useful in defining population break points. Q–Q plots of the Au, As, Cu, and Mo datasets (Fig. 4) show that presence of multiple populations in individual datasets, indicates a mixed origin due to various geological events or process (Zuo et al. 2009, 2012). Thus, Au, As, Cu, and Mo concentrations can be best described by fractal and multifractal modeling.

The zone A and zone B (Fig. 3) were gridded by 20×20 and 50×50 m cells, respectively. Since the fundamentals of C–A fractal method is based on the existence of partition function, and the sampled data cannot be applied effectively; also, inasmuch sampling from the entire study area may not be possible, gridding of the area is inevitably a desired mandate
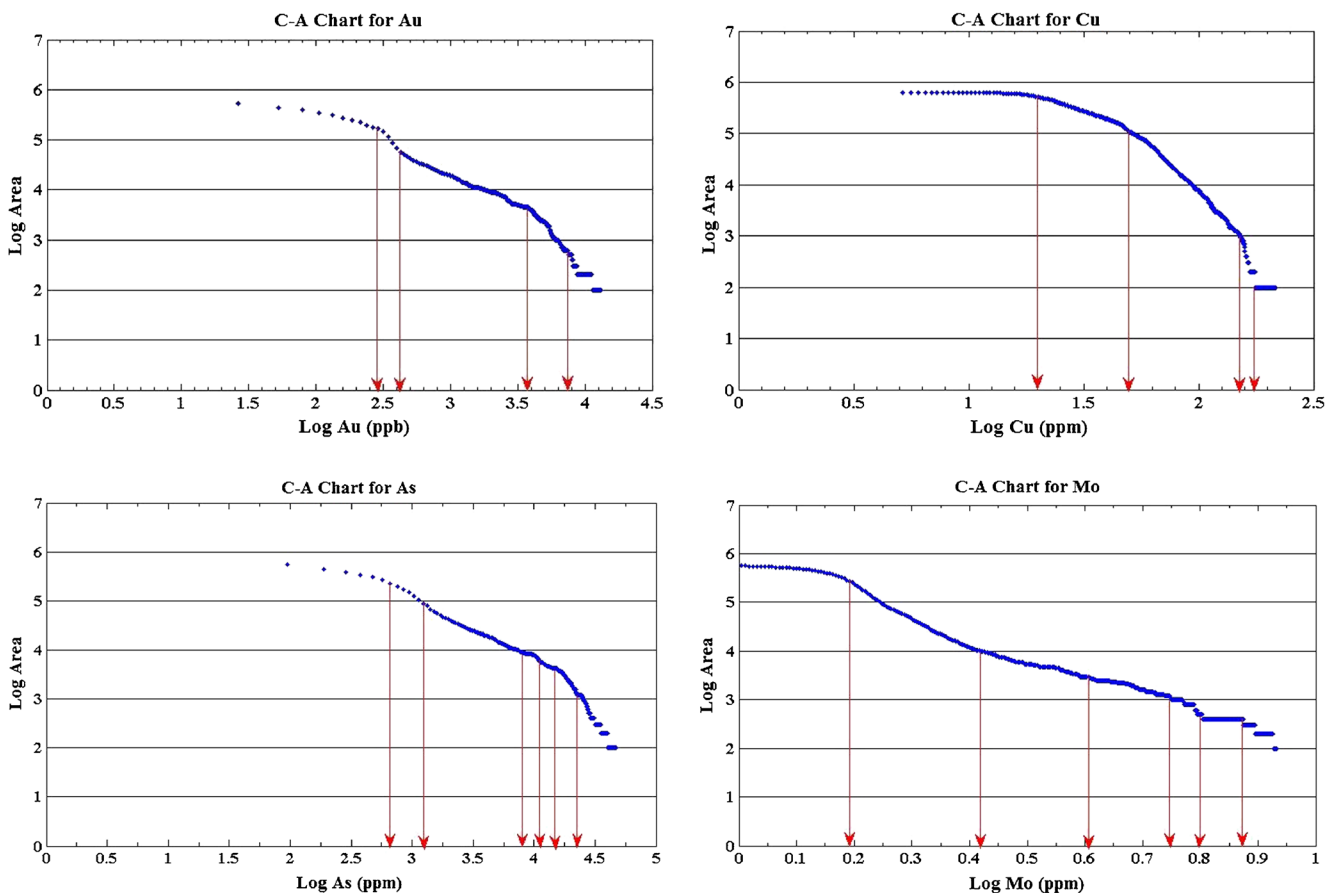

Fig. 5 Log–log plots (C–A method) for Au, As, Cu, and Mo. The vertical axis represents cumulative cell areas $A(\rho)$, with elemental concentration values greater than ρ, and the horizontal axis is the actual value (ρ)

for evaluation and estimation of any parameter, i.e., ore grade. With having a cell characterization in the area we can find and calculate the area which has a certain ore grade and so the problem of over sampling will not enter into picture because the C–A fractal method will automatically eliminate any probable grid related problem in division of the area into smaller elements and the original fractal character is preserved (Evertz and Mandelbrot 1992; Cheng et al. 1994).

Concentration–area relations were computed by assigning an area of influence to each sampled point and summing all elemental areas whose concentration lies below a given value. This procedure was repeated for different elemental concentrations. The evaluated

grades in cells were sorted out based on decreasing grades, and log–log plots were generated for Au and Cu (Fig. 5). Break points between straight-line segments in those log–log plots show threshold values separating populations of geochemical concentration values representing geological differences due to distinct geochemical processes. Elemental geochemical populations are delineated in these log–log plots. On the basis of this procedure, there are five populations for Au and Cu; and seven populations for As and Mo respectively, as depicted in Fig. 5. As shown in C–A log–log plots in Fig. 5, Au anomalous threshold is about 281 ppb and its high-intensity anomaly is 13,280 ppb. According to this
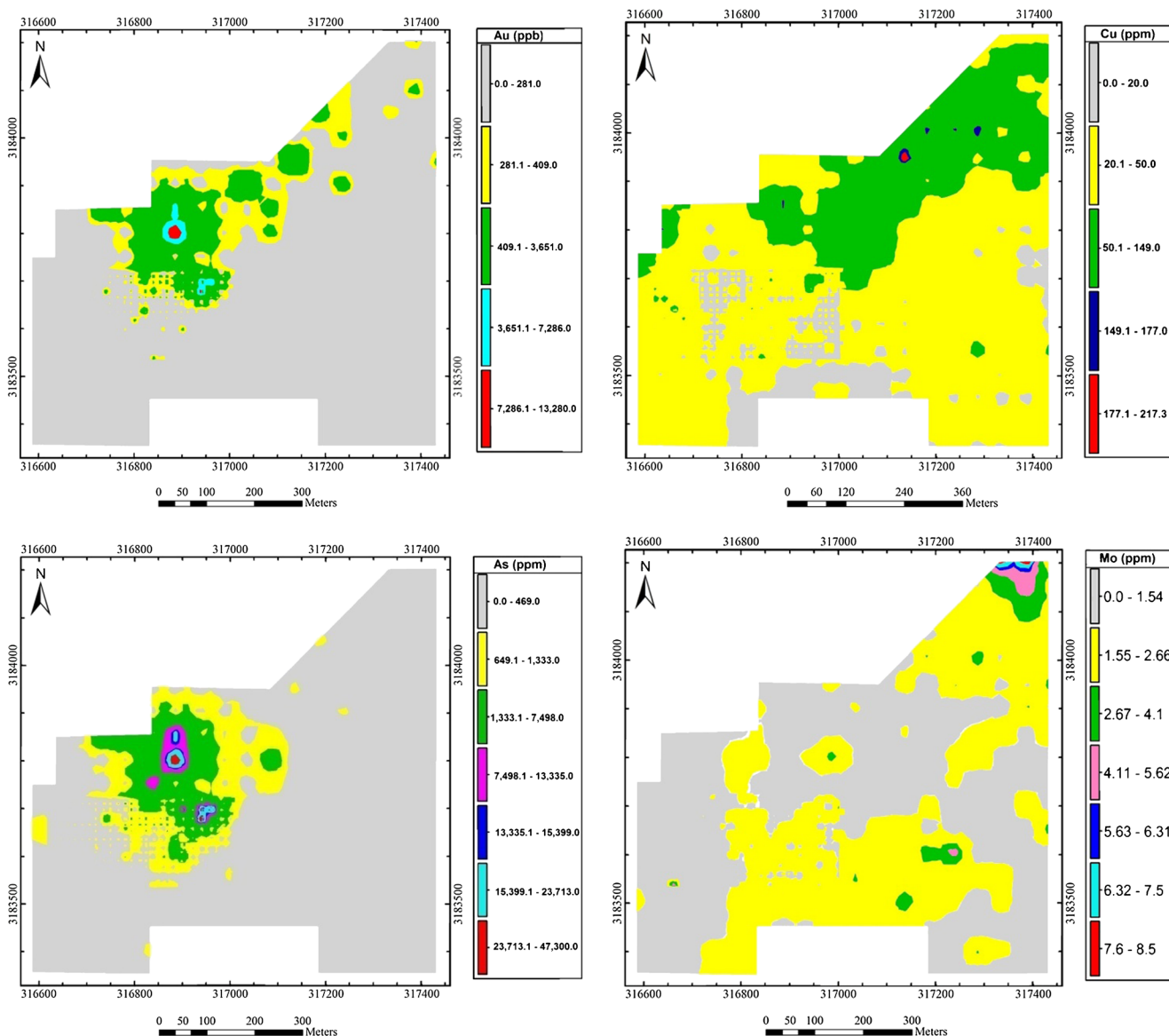

Fig. 6 Au, As, Cu, and Mo geochemical population distribution maps based on C–A method

figure, there are three stages of Au enrichments which the first one started from grades below 409 ppb. Major Au enrichment started from 409 ppb, and 3651 ppb concentration is the beginning of the high-intensity Au anomaly. The final Au mineralization befalls in grades higher than 3651 ppb. As threshold anomalies are 649 ppm (Fig. 5). As log–log plot shows that major As enrichment occurred at 1333 ppm and higher. Cu log–log plot shows that anomalous Cu threshold is about 20 ppm and the first event of Cu enrichment occurred at grades below 50 ppm. The second event shows up between grades 50 and 149 ppm. The final Cu enrichment is in grades higher than 149 ppm. Mo log–log plot shows that major Mo enrichment occurred at 6 ppm and higher.

For each of geochemical population, various kinds of distribution are supposed, and different components, such as chemical elements and their concentrations can be fitted into a straight line on log–log plot. If elements with non-uniform behavior area plotted on log–log coordinates, the plot will have different slopes and various straight-line segments which area connects at an angle or with breaks on the plot. Breaks between the straight-line segments and the corresponding values of Au, As, Cu, and Mo have been used as cut-offs to reclassify distribution maps.

Geochemical maps of the elements were generated by RockWorks™ v.2006 software package. Based on the results of the C–A method, elemental-grade distribution maps were drawn and are presented in Fig. 6. According to these maps,
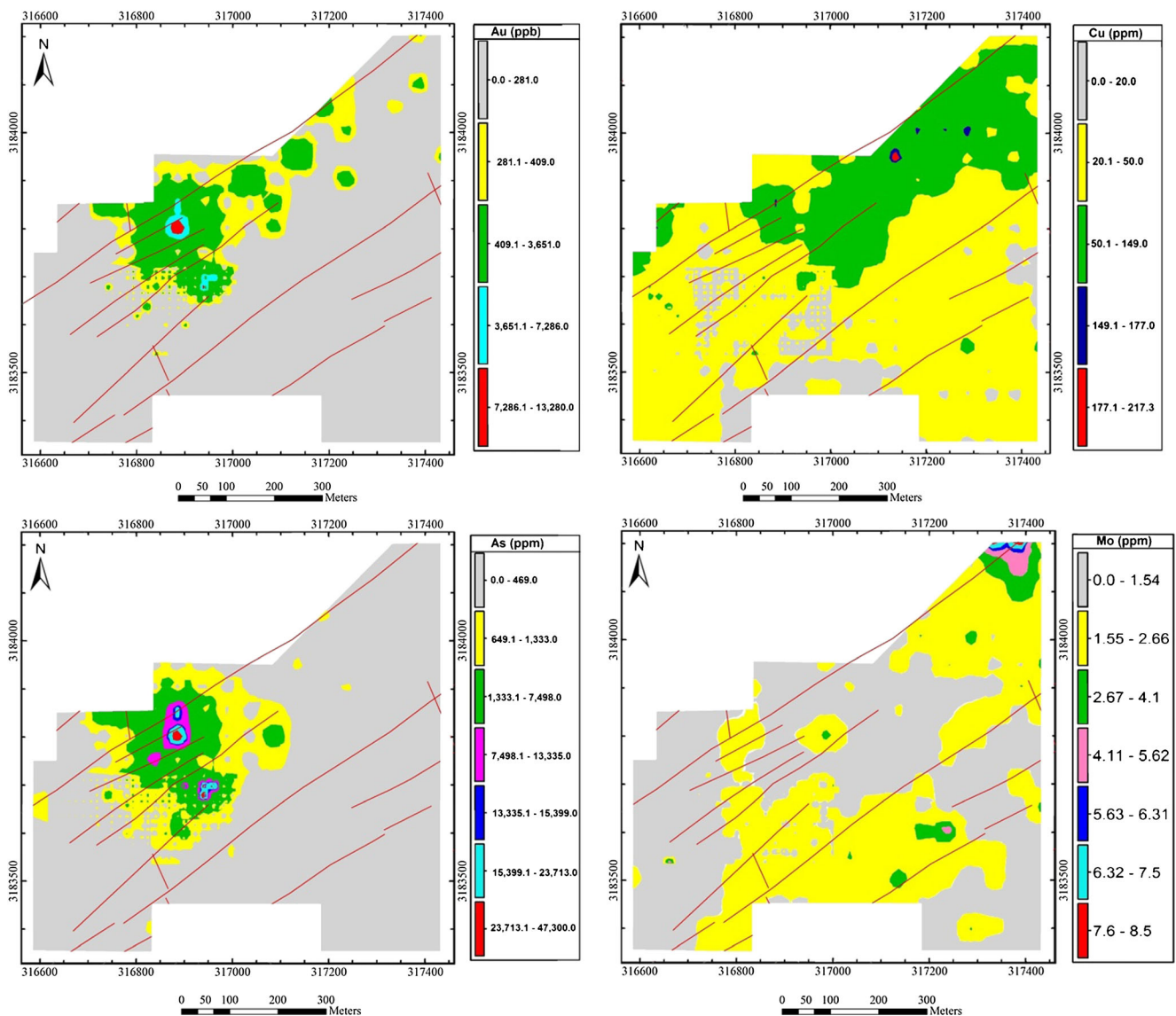

Fig. 7 Relationship between Au, As, Cu, and Mo geochemical population distribution maps based on the C–A method imposed on fault location maps (red lines)
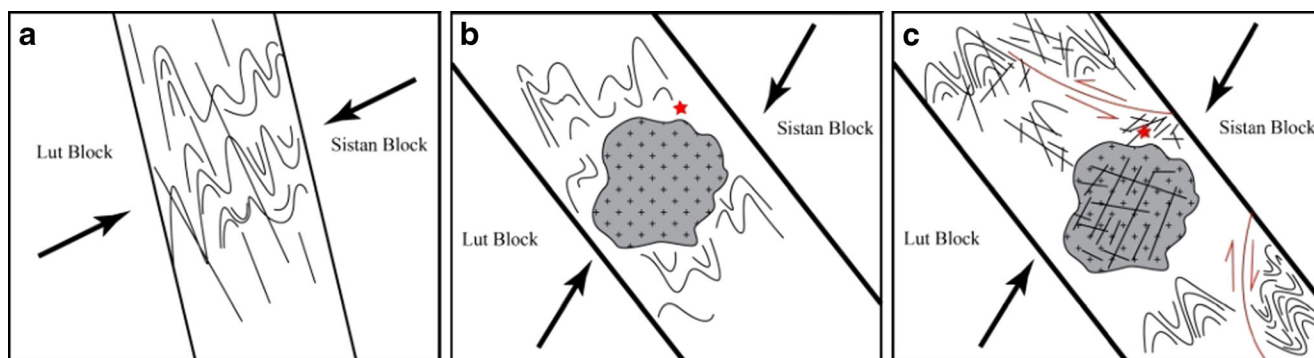
Fig. 8 Schematic sketch of the tectonic evolution in east of Iran

most of Au anomalies are located in western and central parts of the area. Corresponding Au and As anomalies indicates association of Au mineralization with As. Several Cu anomalies are interpreted in central and northeastern parts of the area. Moreover, Mo anomalies were situated in northeastern parts and are small.

Comparison with geological particulars

To separate major mineralized zones, specific geological particulars including the faults and alterations have been correlated with thresholds and cut-off results from C–A method. Au, As, Cu, and Mo distributions and faults map in the Siah-Jangal area are shown in Fig. 7. Comparison between fault positions and elemental anomalies shows that faults intersect the anomalies situated near those structures (Fig. 7). On the other hand, faults and elemental anomalies have a proportional relationship. High-grade elemental anomalies occurred inside and within the fault zones or situated on faults intersection areas (Fig. 7). This is a positive parameter because silicified and quartz-sulfide veins occurred along these faults, and Au particles existed in these veins and veinlets.

It can be deduced that fault density has a direct positive correlation with Au mineralization especially in the central parts of the study area.

Thick sequences of Eocene turbidities and remnants of the upper Cretaceous ophiolitic rocks were trapped in the sistan suture zone. These sequences have been folding and faulting as large folds with the NW trending axial plane during the closure of the Sistan Ocean (Fig. 8a). Continuity of convergence between the two blocks on both sides of the mentioned ocean (the Lut Block in the west and the Sistan Block in the east) has provided several NW and NE conjugate fracture zones in this region. With the onset of the subduction, Oman oceanic lithosphere beneath the southern margin of the

Makran zone, Taftan magmatism as the large plutonic bodies, has interrupted these sequences (Fig. 8b). Reciprocally, compression of Arabic plate to Eurasian plate caused considerable shortening in the East of Iran. Moreover, these compressional movements reactivated the two shear systems that called NW left-lateral strike-slip JunAbad fault system and NE right-lateral strike-slip Saravan fault system, which causes changes in the sistan suture zone (Figs. 8c and 9). Magmatic activities during and after these tectonic events could have an important role in mineralization of the study area.

One main rock type—diorite—is present in the study area. Pyrite-rich diorite porphyry igneous rocks have infiltrated into flysh units and cause the various alterations zones. These alteration zones also have a strong positive relationship with Au, As, and Cu anomalies. All of the anomalous parts are covered by argillic and advance argillic alterations. Argillic alteration units are
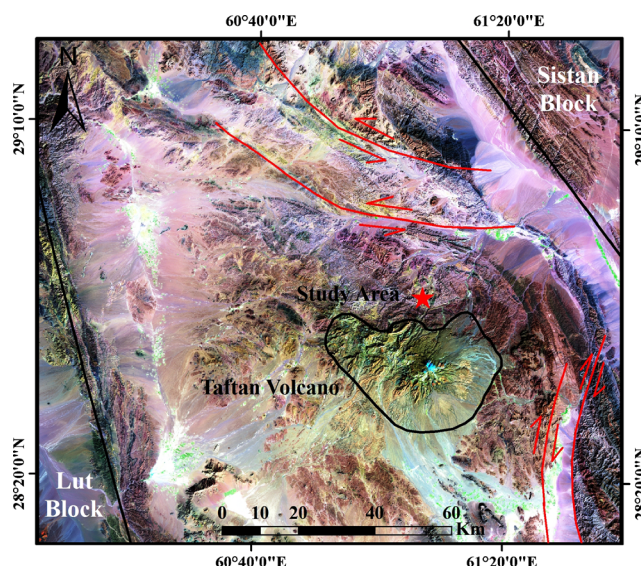

Fig. 9 Landsat 7 ETM$^+$ image for the east of Iran

widespread in central and south parts of the study area. Argillic alteration is associated with high intensive Au, As, Cu, and Mo as shown in Fig. 10. Au concentrations higher than 409 ppb, As concentrations higher than 1333 ppm, and Cu concentrations higher than 50 ppm are anomalies in central and northeastern parts of the area. A small part of high-intensity Mo anomaly (2–5 ppm) in the northeastern parts of the area is covered by argillic alteration as well.

Advanced argillic alteration zones mostly are situated in the central and northeastern parts of the Siah-Jangal area (Fig. 11). Argillic and advance argillic alterations zones are correlated with the higher intensity of Au anomalies (over 1000 ppb) in the central part of the area. Anomalous
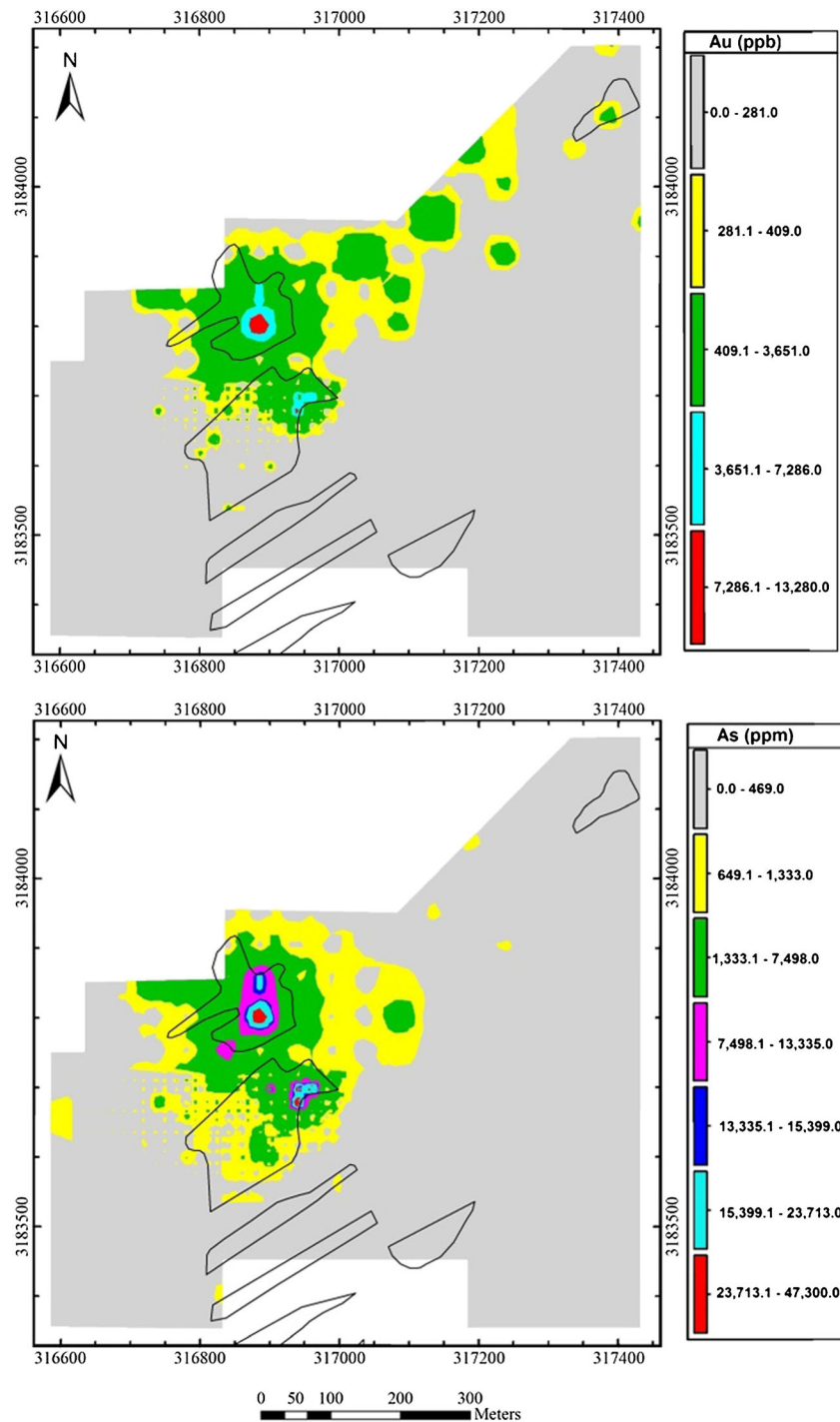

Fig. 10 Relationship between Au, As, Cu, and Mo anomalies and argillic alteration zone (*black polygons*)
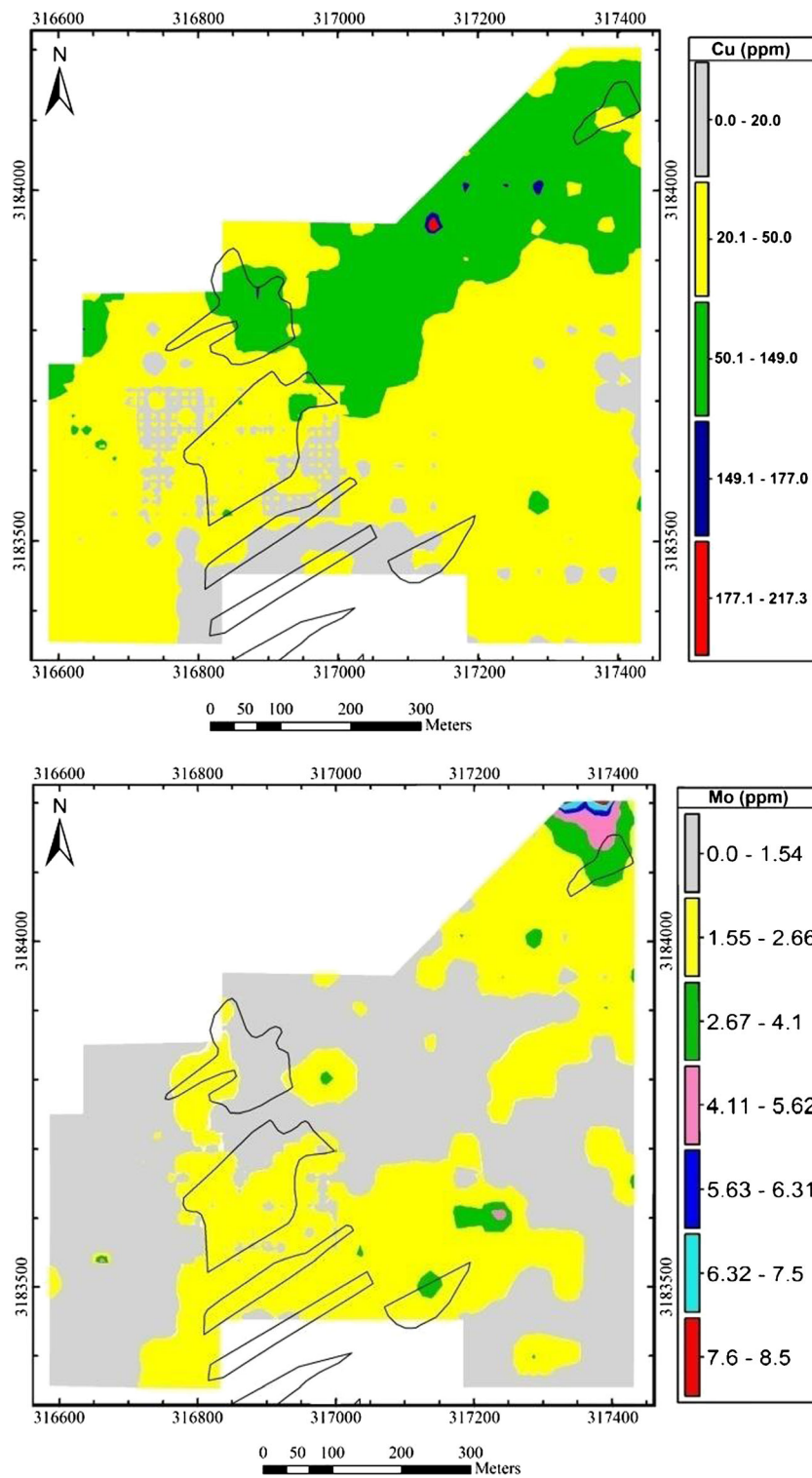
Fig. 10 (continued)

parts of Au have a rather good relationship with these units (Figs. 8 and 9). Moreover, advanced argillic alterations is related to the richest Cu anomaly in northeastern parts of the study area but these anomalies are located outside of most Au and As bearing anomalies as depicted in Fig. 11. Mo anomalies in the northeastern parts, between 4 and 8 ppm, of the area show a rather good relationship with this alteration zones (Fig. 11).
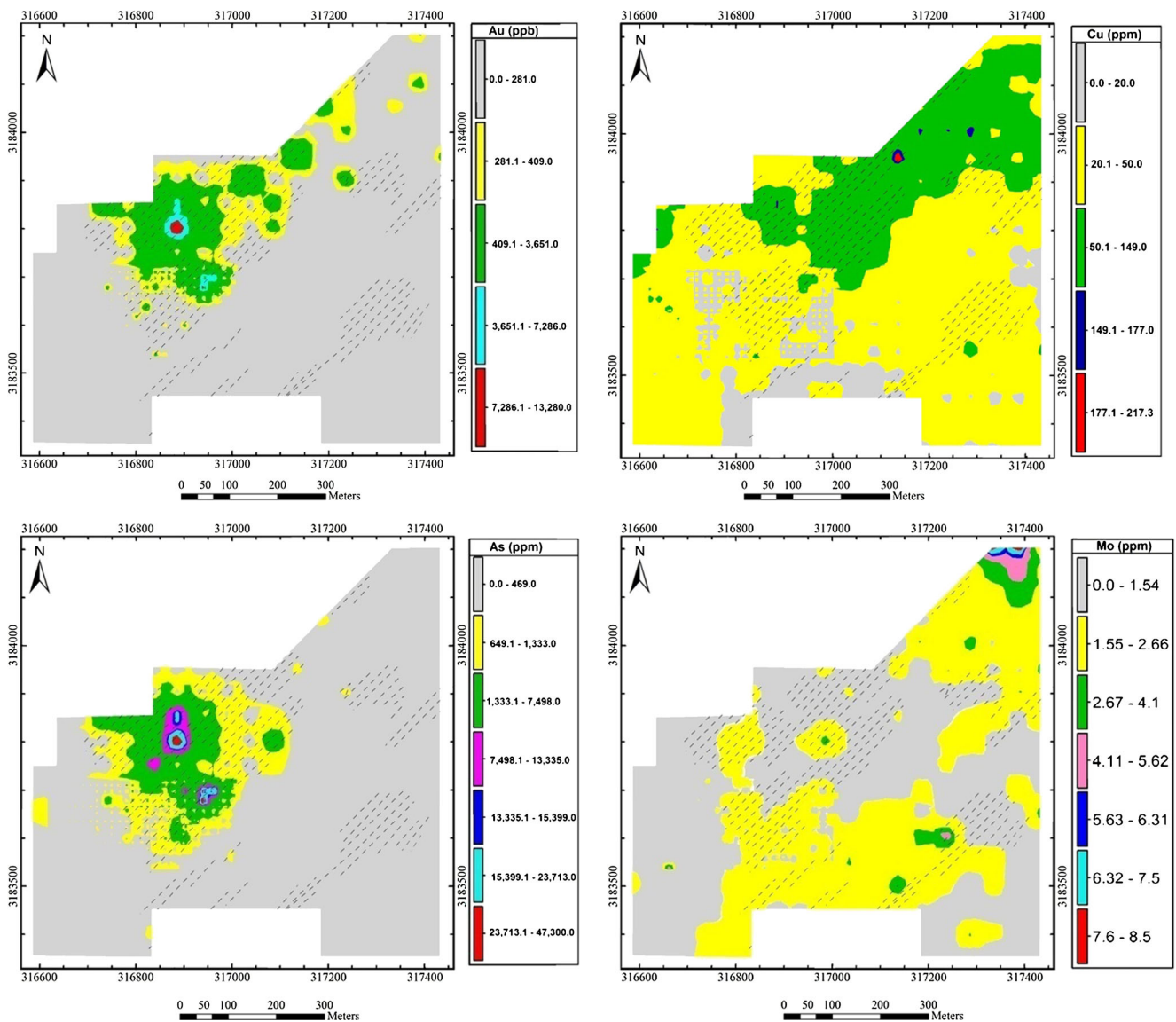
Fig. 11 Relationship between Au, As, Cu, and Mo anomalies and advance argillic alteration zone (*dashed lines*)

Conclusion

This study conducted at the Siah-Jangal Au porphyry deposit presents the spatial use of the C–A method for geochemical anomaly separation as useful tool for geochemical and mineral exploration. The advantage of this method relies essentially in its simplicity, and easy computational implementations, as well as the possibility of computing a numerical value of concentration (i.e., the anomalous threshold), which is the most useful criteria for cross-information with numerical data from different sources, commonly used in lithogeochemistry studies.

Based on the threshold obtained from C–A method, the Au, As, and Cu concentrations can be divided into several concentration segment populations, each of which is generally distributed in the area dominated by a single type of geologic

event. Interpretation of C–A log–log plots of Au and Cu shows that Au and Cu concentrations in the area may be a result of the three steps of enrichment, i.e., mineralization and later dispersions.

The studied element anomalies have proper and direct relationships with faults in Siah-Jangal area. High intensive element anomalies are mostly situated at fault intersections. These kinds of occurrence are seen especially in the center of the area. Moreover, there is a good correlation between argillic/advance argillic alterations and anomalous concentration, of Au, As, Cu, and Mo. Low to high intensive argillic alterations zones have a good relationships with high-grade anomalous elemental enrichment parts in the central part of the area, specifically for Au and As elements.

Furthermore, geological evidences include alterations and tectonics setting proved that accuracy of the results is obtained

from C–A methods. The richest parts of these elements correlated with the direction to tectonic and alteration units which are situated at fault intersections. This event shows that high-grade mineralizations of these elements are controlled by tectonics and fluid flows.

The multifractal nature of C–A log–log curves could be of essential help to geoscientists for interpreting the stages at which an element is enriched. The developments in multifractal theory and their usage could provide a favorable ground for the stochastic simulation of geochemical distributions and their understanding and interpretations. We propose to continue our lithogeochemical studies in the north and northwestern of the area to estimate the anomaly trends especially with regard to Au and Cu.

References

Afzal P, Khakzad A, Moarefvand P, Rashidnejad Omran N, Esfandiari B, Fadakar Alghalandis Y (2010) Geochemical anomaly separation by multifractal modeling in Kahang (Gor Gor) porphyry system, Central Iran. J Geochem Explor 104:34–46

Afzal P, Fadakar Alghalandis Y, Khakzad A, Moarefvand P, Rashidnejad Omran N (2011) Delineation of mineralization zones in porphyry Cu deposits by fractal concentration–volume modeling. J Geochem Explor 108:220–232

Afzal P, Dadashzadeh Ahari H, Rashidnejad Omran N, Aliyari F (2013) Delineation of gold mineralized zones using concentration–volume fractal model in Qolqoleh gold deposit. NW Iran Ore Geol Rev 55:125–133

Afzal P, Alhoseini SH, Tokhmechi B, Kaveh Ahangaran D, Yasrebi AB, Madani N, Wetherelt A (2014) Outlining of high quality coking coal by concentration–volume fractal model and turning bands simulation in East-Parvadeh coal deposit, Central Iran. Int J Coal Geol 127:88–99

Agterberg FP, Cheng Q, Brown A, Good D (1996) Multifractal modeling of fractures in the Lac du Bonnet batholith, Manitoba. Comput Geosci 22(5):497–507

Arias M, Gumiel P, Martin-Izard A (2012) Multifractal analysis of geochemical anomalies: a tool for assessing prospectivity at the SE border of the Ossa Morena zone, Variscan Massif (Spain). J Geochem Explor 122:101–112

Berberian F, Muir I, Pankhurst R, Berberian MN (1982) Late cretaceous and early Miocene Andyan-type plutonic activity in northern Makran and central Iran. J Geol Soc Lond 139:605–614

Bolviken B, Stokke PR, Feder J, Jossang T (1992) The fractal nature of geochemical landscapes. J Geochem Explor 43:91–109

Carranza EJM (2008) Geochemical anomaly and mineral prospectivity mapping in GIS, handbook of exploration and environmental geochemistry. Elsevier, Amsterdam

Carranza EJM (2009) Controls on mineral deposit occurrence inferred from analysis of their spatial pattern and spatial association with geological features. Ore Geol Rev 35:383–400

Chen Y, Zhao P, Chen J, Liu J (2001) Application of the geo-anomaly unit concept in quantitative delineation and assessment of gold ore targets in Western Shandong Uplift Terrain, Eastern China. Nat Resour Res 10:35–49

Cheng QM (1999) Spatial and scaling modeling for geochemical anomaly separation. J Geochem Explor 63(3):175–194

Cheng Q (2000) Geo Data Analysis System (GeoDAS) for mineral exploration: user's guide and exercise manual. Material for the training workshop on GeoDAS held at York University, Toronto, Canada vol.1, 3, p. 204

Cheng Q (2007) Mapping singularities with stream sediment geochemical data for prediction of undiscovered mineral deposits in Gejiu, Yunnan Province. China Ore Geol Rev 32:314–324

Cheng Q (2008) Non-linear theory and power–law models for information integration and mineral resources quantitative assessments. Math Geosci 40:503–532

Cheng Q (2012) Singularity theory and methods for mapping geochemical anomalies caused by buried sources and for predicting undiscovered mineral deposits in covered areas. J Geochem Explor 122:55–70

Cheng Q, Agterberg FP (1996) Multifractal modeling and spatial statistics. Math Geol 28(1):1–16

Cheng Q, Agterberg FP, Ballantyne SB (1994) The separation of geochemical anomalies from background by fractal methods. J Geochem Explor 51:109–130

Deng J, Wang Q, Yang L, Wang Y, Gong Q, Liu H (2010) Delineation and explanation of geochemical anomalies using fractal models in the Heqing area, Yunnan Province, China. J Geochem Explor 105:95–105

Ellouz-Zimmermann N, Lallemant SJ, Castilla R, Mouchot N, Leturmy P, Battani A et al (2007) Offshore frontal part of the Makran accretionary prism (Pakistan): the Chamak survey. In: Lacombe O, Lavé J, Roure F, Vergés J (eds) Thrust belts and foreland basins: from fold kinematics to hydrocarbon systems: Berlin. Springer-Verlag, Heidelberg, pp 349–363

Evertz CJG, Mandelbrot BB (1992) Multifractal measures (appendix B). In: Peitgen H-O, Jurgens H, Saupe D (eds) Chaos and fractals. Springer, New York

Farhoudi G, Karige DE (1997) Makran of Iran and Pakistan as an active arc system. Geology 5(11):664–668

Ford A, Blenkinsop TC (2008) Evaluation geological complexity and complexity gradients as control on copper mineralization, Mt Isa In lier. Aust J Earth Sci 55:13–23

Goncalves MA, Vairinho M, Oliveira V (1998) Study of geochemical anomalies in Mombeja area using a multifractal methodology and geostatistics. In: Buccianti A, Nardi G, Potenza R (eds) IV IAMG'98. De Frede, Ischia Island, pp 590–595

Goncalves MA, Mateus A, Oliveira V (2001) Geochemical anomaly separation by multifractal modeling. J. Geochem. Explor 72, 91–114.

Grando G, McClay K (2007) Morphotectonic domains and structural styles in the Makran accretionary prism, offshore Iran. Sediment Geol 196:157–179

Grunsky E, Smee B (1999) Differentiation of soil types and mineralization from multielement geochemistry using multivariate methods and digital topography. J Geochem Explor 67(1–3):289–302

Gumiel P, Sanderson DJ, Arias M, Roberts S, Martín-Izard A (2010) Analysis of the fractal clustering of ore deposits in the Spanish Iberian Pyrite Belt. Ore Geol Rev 38:307–318

Harris JR, Wilkinson L, Grunsky G, Heather K, Ayer J (1999) Techniques for analysis and visualization of lithogeochemical data with applications to the Swayze greenstone belt, Ontario. J Geochem Explor 67:301–334

Harris JR, Grunsky EC, Wilkinson L (2000) Effective use and interpretation of lithogeochemical data in regional exploration programs. Ore Geol Rev 16:107–143

Hashemi M, Afzal P (2013) Identification of geochemical anomalies by using of number–size (N–S) fractal model in Bardaskan area, NE Iran. Arab J Geosci 6(12):4785–4794

Hassanpour S, Afzal P (2011) Application of concentration–number (C–N) multifractal modeling for geochemical anomaly separation in Haftcheshmeh porphyry system NW Iran. Arab J Geosci. doi:10.1007/s12517-011-0396-2

Kavoshgaran Consulting Engineers Company (2003) Poly-metal exploration in the Chahoun-Siahhangal area. Research Institute and Application of minerals in Iran

Kavoshgaran Consulting Engineers Company (2006) Final report, preliminary exploration of gold in the Siah-jangal area. Research Institute and Application of Minerals in Iran

Li Q, Cheng Q (2004) Fractal singular-value (eigen-value) decomposition method for geophysical and geochemical anomaly reconstruction. Earth Sci-China Univ, Geosci 29:109–118, In Chinese with English Abstract

Li C, Ma T, Shi J (2003) Application of a fractal method relating concentrations and distances for separation of geochemical anomalies from background. J Geochem Explor 77:167–175

Lima A, De Vivo B, Cicchella D et al (2003) Multifractal IDW interpolation and fractal filtering method in environmental studies: an application on regional stream sediments of (Italy). Campania Reg Appl Geochem 18:1853–1865

Lima A, De Vivo B, Tarvainen T et al (2008) Interpolation methods for geochemical maps: a comparative study using arsenic data from European stream waters. Geochem Explor Environ Anal 8:41–48

Mandelbrot BB (1983) The fractal geometry of nature. W. H. Freeman, San Fransisco, p 468

Mehrpartoo M, Padiar F (2003) Geological map of Taftan, 1:100,000 Series. Geological Survey of Iran, Tehran

Pazand K, Hezarkhani A, Ataei M, Ghanbari Y (2011) Application of multifractal modeling technique in systematic geochemical stream sediment survey to identify copper anomalies: a case study from Ahar, Azarbaijan, Northwest Iran. Chem Erde 71:397–402

Perello J, Razique A, Schloderer J, Rehman A (2008) The chagai porphyry copper belt, Baluchistan

Rafiee A (2005) Separating geochemical anomalies in stream sediment media by applying combination of fractal concentration–area model and multivariate analysis (Case study: Jeal-e-Barez 1:100,000 Sheet, Iran). 20th World Mining Congress Proceeding, Iran, pp. 461–470

Rowan L, Schmidt R, Mars J (2006) Distribution of hydrothermally altered rocks in the Reko Diq, Pakistan mineralized area based on spectral analysis of ASTER data. Remote Sens Environ 104:74–87

Shapiro SS, Wilk MB (1965) An analysis of variance test for normality (complete samples). Biometrika 52:591–611

Sim BL, Agterberg FP, Beaudry C (1999) Determining the cutoff between background and relative base metal contamination levels using multifractal methods. Comput Geosci 25:1023–1041

Singer DA, Kouda R (2001) Some simple guides to finding useful information in exploration geochemical data. Nat Resour Res 10:137–147

Taghizadeh N (1996) Reports of prospections in Baluchestan,. Geological survey of Iran, Internal Repts, 1996

Tirrul R, Bell I, Griffis R, Camp V (1983) The Sistan Suture zone of eastern Iran. Geol Soc Am Bull 94:134–150

Turcotte DL (1997) Fractals and chaos in geology and geophysics. Cambridge University Press, Cambridge

Wang G, Carranza EJM, Zuo R, Hao Y, Yangsong D, Pang Z, Qu J (2012) Mapping of district-scale potential target using fractal models. J Geochem Explor 122:34–46

Wei S, Pengda Z (2002) Theoretical study of statistical fractal model with applications to mineral resource prediction. Comput Geosci 28:369–376

Zarcan Minerals I.N.C. June Company (2003) Final report of Balouchestan exploration project on exploration and base line date studies for selected areas to be retained. Vancover, Canada: Eds. Baker, E. and Reimchen, T.H.F

Zuo R (2011) Decomposing of mixed pattern of arsenic using fractal model in Gangdese belt, Tibet. China Appl Geochem 26:S271–S273

Zuo R, Cheng Q, Xia Q (2009) Application of fractal models to charactrization of vertical distribution of geochemical element concentration. J Geochem Explor 102:37–43

Zuo R, Carranza EJM, Cheng Q (2012) Fractal/multifractal modelling of geochemical exploration data. J Geochem Explor 122:1–3